THE EFFECTS OF INCLINATION ANGLE AND PRANDTL NUMBER ON THE MIXED CONVECTION IN THE INCLINED LID DRIVEN CAVITY USING LATTICE BOLTZMANN METHOD

ARASH KARIMIPOUR

Department of Mechanical Engineering, Najafabad Branch, Islamic Azad University, Isfahan, Iran

e-mail: arashkarimipour@gmail.com

ALIREZA HOSSEIN NEZHAD

University of Sistan and Baluchestan, Department of Mechanical Engineering, Zahedan, Iran

e-mail: nezhadd@hamoon.usb.ac.ir

ANNUNZIATA D'ORAZIO

Dipartimento di Ingegneria Astronautica, Elettrica ed Energetica, Sapienza Università di Roma, Rome, Italy

e-mail: annunziata.dorazio@uniroma1.it

EBRAHIM SHIRANI

Foolad Institute of Technology, Fooladshahr, Esfahan, Iran

e-mail: eshirani@ictp.it

The laminar mixed convection in a two-dimensional rectangular inclined cavity with moving top lid is investigated using the double population thermal lattice Boltzmann method (LBM) at different values of the Richardson number, inclination angle and the Prandtl number. In this problem, velocity components are changed by both buoyancy forces and the inclination angle of the cavity. Comparison of the present results with other available data shows good agreement. As the results, the velocity and temperature profiles, the Nusselt number, streamlines and isotherms are presented and discussed. It is shown that the increase of Prandtl number enhances the heat transfer rate, especially at higher values of inclination angle and Richardson number. Moreover, the average Nusselt number at the upper limit of the considered range of the Richardson and Prandtl numbers variability increases by a factor of 9.

Key words: LBM, inclination angle, Prandtl number, mixed convection

Nomenclature

AR	–	cavity aspect ratio (L/H)
c_s, e	–	lattice speed of sound and internal energy
f, g	–	momentum and internal energy functions
f^e, g^e	–	equilibrium distribution functions
$\mathbf{g}$	–	gravity vector
$\mathrm{Gr}, \mathrm{Ma}, \mathrm{Pr}$	–	Grashof, Mach and Prandtl number, respectively
H, L	–	height and length of the cavity
k	–	thermal conductivity
Nu_m	–	average Nusselt number
$\mathbf{q}$	–	heat flux
R	–	constant of gas
$\mathrm{Ra}, \mathrm{Re}, \mathrm{Ri}$	–	Rayleigh, Reynolds and Richardson number, respectively
t, T	–	time and temperature, respectively
T_c, T_h	–	cold and hot wall temperature

$\mathbf{u}$	–	macroscopic flow velocity vector, $\mathbf{u} = [u, v]$
U_0	–	top lid velocity
(U, V)	–	dimensionless flow velocity, $(U, V) = (u/U_0, v/U_0)$
U_w, V_w	–	velocity components of the cavity walls
$\mathbf{x}$	–	dimensional Cartesian coordinate vector, $\mathbf{x} = (x, y)$
(X, Y)	–	dimensionless coordinates, $(X, Y) = (x/H, y/H)$
Z	–	viscous heating term

Greek symbols

α	–	thermal diffusivity	ν	–	kinematic viscosity
β	–	volumetric expansion coefficient	θ	–	dimensionless temperature,
ρ	–	density			$\theta = (T - T_c)/(T_h - T_c)$
γ	–	cavity inclination angle	τ_f, τ_g	–	relaxation times

1. Introduction

The lattice Boltzmann method is a particle based approach being used for the numerical simulation of fluid flow and heat transfer. The particle characteristic of this method has increased its application in a wide range of fluid flow and heat transfer problems, so that in addition to the simulation of macroflows (Grucelski and Pozorski, 2012; Kefayati *et al.*, 2011; Nemati *et al.*, 2010; Yang and Lai, 2011), it is used for the simulation of micro and nano flows (Kandlikar *et al.*, 2006; Karimipour *et al.*, 2012; Niu *et al.*, 2007; Tian *et al.*, 2010). Moreover, LBM has found wide application in micro-electro-mechanical-systems (MEMS) and nano-electro-mechanical systems (NEMS). Compared to the conventional numerical methods and other particle based simulations such as molecular dynamics simulation and direct simulation Monte Carlo, LBM is more appropriate for parallel processing. Moreover, using LBM, the pressure field is directly calculated without the need for solving another system of equations, multiphase and complex flows can be solved easier, and less computational memory and time are needed (Chen *et al.*, 1992; Chen and Doolen, 1998; Oran *et al.*, 1998). Moreover, LBM consists of only first-order PDEs, which makes discretization and programming simpler than Navier-Stokes equations which are second-order PDEs. Moreover, the nonlinear convective term in Navier-Stokes equations is written simpler in LBM (Tallavajhula *et al.*, 2011). These advantages give incentives to researchers to study the application of the LBM to solve more realistic problems by improving and innovating the LBM models and related boundary conditions. However, there are some difficulties and drawbacks in LBM: it is a compressible model for ideal gas, and theoretically always simulate the compressible Navier-Stokes equation. However, the incompressible Navier-Stokes equations can be derived from the LBM through the Chapman-Enskog expansion at the nearly incompressible limit. It means LBM can simulate an incompressible flow under low Mach number (Ma < 0.15). The compressible nature of LBM produces a compressibility error, which at low values of the Mach number will be negligible (order of Ma^2) (Buick and Greated, 2000; He and Luo, 1997; Mohamad, 2011; Shi *et al.*, 2006). Moreover, the LBM multi phase model can not simulate the systems with large viscosity ratio fluids (Kuzmin and Mohamad, 2009). In addition, using the regular square grids is another difficulty of LBM for simulation of the curved boundaries. Some researchers have dealt with curved boundaries and using unstructured meshes in LBM (Cheng and Hung, 2002; Kao and Yang, 2008; Peng *et al.*, 1999). Kao and Yang (2008) applied an interpolation-based approach (under a uniform Cartesian mesh) to track the position of boundary for solving the distribution functions near the curved boundary. This method results in a loss of mass conservation and reduces the accuracy at the boundary. Ubertini and Succi (2008) used non-uniform or unstructured meshes for LBM to improve both stability and accuracy. However, they reported that further improvements are necessary to obtain accurate results at

different flow conditions. To simulate heat transfer, different lattice Boltzmann methods have been proposed such as the multi-speed, passive scalar, and doubled populations internal energy method. The last method has been widely used to simulate natural convection problems (He *et al.*, 1998). Guo *et al.* (2007) used thermal LBM for solving low Mach number thermal flows with viscous dissipation and compression work. They obtained a lattice Boltzmann equation model from a kinetic model for the decoupled hydrodynamic and energy equations. Their model was tested by simulating the thermal Poiseuille flow in a planer channel and natural convection in a square cavity. Natural convection in the inclined cavity using LBM has been reported in various articles in the recent years (Jafari *et al.*, 2011; Mezrhab *et al.*, 2006). Numerous investigations have been conducted in the past on the lid-driven cavity flow and heat transfer, considering various combinations of the imposed temperature gradients and cavity configurations. Sharif (2007) studied numerically two-dimensional shallow rectangular driven cavities of aspect ratio $AR = 10$ for Ra ranging from 10^5 to 10^7, keeping the Reynolds number fixed at Re = 408.21. Basak *et al.* (2009) performed finite element simulations to investigate the influence of linearly heated side wall(s) or cooled right wall on mixed convection lid-driven flows in a square cavity. Sivasankaran *et al.* (2010) performed a numerical study, with the finite volume method, on mixed convection in a lid-driven cavity with vertical sidewalls maintained with sinusoidal temperature distribution and top and bottom wall adiabatic; the results were analyzed over a range of Ri, amplitude ratios and phase deviations. The amplitude ratio was defined as the ratio of the amplitude of temperature oscillations of the right wall to that of the left wall, and the phase deviation was defined as the phase difference of temperature oscillations between the right and left walls. The effects of Prandtl numbers $(0.7 < \text{Pr} < 70)$ on natural convection in the cavity using LBM were investigated by Kao and Yang (2007). Satisfying the nearly incompressible flow $(\text{Ma} < 0.1)$, they determined different characteristic velocities at each Pr. Their approach showed good performance at Pr = 0.7 and Pr = 7; however, it needed more time at higher Pr values. Their method is usually applied for $\text{Pr} \leqslant 7$ (Nemati *et al.*, 2010). Parmigiani *et al.* (2009) used two supplementary methods for higher values of Pr and Ra $(10 < \text{Pr} < 10^4$ and $10^4 < \text{Ra} < 10^9)$ to simulate natural convection using LBM. In their first method, the timescales of thermal and density-momentum distribution functions are separated at higher Pr values. In their second method, a smaller grid size is used for the thermal distribution function than for the density-momentum distribution function. Simulation of mixed convection using LBM at different conditions has been one of the interesting topics for researchers in the recent years (Guo *et al.*, 2010; Du *et al.*, 2011; Fattahi *et al.*, 2011). Among them, Rosdzimin *et al.* (2010) studied the effects of a heated square inside the lid driven cavity, using the nine-velocity model for the velocity field and the four-velocity model for the thermal field.

The mentioned review shows that mixed convection in an inclined lid driven cavity has not been investigated by LBM. So, in this work, for a laminar mixed convection, the effects of *gamma* and Pr at different Ri values on the thermal and hydrodynamic fluid properties inside a two-dimensional inclined enclosure with hot moving top lid are studied.

2. Problem statement

The fluid mixed convection inside an enclosure shown in Fig. 1 ($L/H = 3$) is studied utilizing LBM. The upper lid temperature is larger than that of the lower wall. U_0 is the upper wall velocity and the side walls are insulated. A computer program in Fortran language is developed to simulate the fluid parameters for $\text{Re} = U_0 H / \nu = 200$ and $\text{Ri} = \text{Gr}/\text{Re}^2 = 0.1, 1, 10$, in which $\text{Gr} = g\beta\Delta T H^3/\nu^2$. The effects of $\gamma = 0°, 30°, 60°, 90°$ and $\text{Pr} = \nu\alpha = 0.07, 0.7, 7$ are studied on heat transfer and fluid flow; ν and α are the kinematic viscosity and thermal diffusivity. LBM is applied in near-incompressible regimes. Thus, in the Mach number definition, $\text{Ma} = U^*/c_s \ll 1$,

the characteristic velocity of the flow for both natural, $U^* = \sqrt{g\beta\Delta TH}$, and forced convection, $U^* = \nu\mathrm{Re}/H$, must be small compared with the speed of sound. The compressibility errors are proportional to Ma^2, so at low values of the Mach number, density variations will be negligible. In the present work, Ma is assumed as 0.1; therefore, the compressibility errors would be negligible.
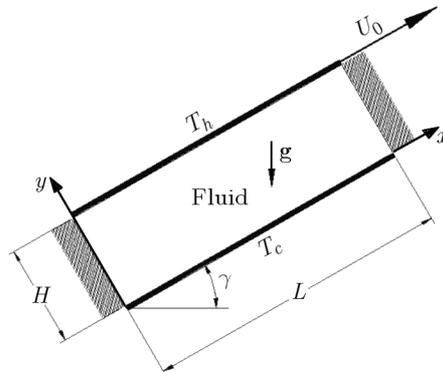

Fig. 1. Inclined cavity geometry and coordinates axis

3. Formulation

3.1. Lattice Boltzmann method

The dimensionless lattice Boltzmann equations for hydrodynamic and thermal models are as follows (He *et al.*, 1998)

$$\frac{\partial f_i}{\partial t} + c_{i\alpha}\frac{\partial f_i}{\partial x_\alpha} = -\frac{f_i - f_i^e}{\tau_f} \qquad \frac{\partial g_i}{\partial t} + c_{i\alpha}\frac{\partial g_i}{\partial x_\alpha} = -\frac{g_i - g_i^e}{\tau_g} - f_i Z_i \tag{3.1}$$

where f_i is the discretised momentum distribution function and denotes the probability density of particles having velocity around $c_{i\alpha}$ at an infinitesimal volume element centered at x_α. g is called the internal energy density distribution function. Indices i and α are lattice velocity directions and x-y geometry components, respectively, τ_f and τ_g are hydrodynamic and thermal relaxation times, respectively, f^e and g^e are hydrodynamic and thermal equilibrium distribution functions, respectively, and $\mathbf{c}_i$ represents microscopic particles velocity. Using D2Q9 lattice (Qian *et al.*, 1992), shown in Fig. 2, the subscript i varies from 1 to 9. So, the microscopic particle velocities are calculated as follows

$$\mathbf{c}_{i=0} = [0,0] \qquad \mathbf{c}_{i=1,2,3,4} = \Big[\cos\frac{i-1}{2}\pi, \sin\frac{i-1}{2}\pi\Big]c$$
$$\mathbf{c}_{i=5,6,7,8} = \sqrt{2}\Big[\cos\Big(\frac{(i-5)\pi}{2}+\frac{\pi}{4}\Big), \sin\Big(\frac{(i-5)\pi}{2}+\frac{\pi}{4}\Big)\Big]c \tag{3.2}$$

Z is the heat dissipation term defined as

$$Z_i = (c_{i\alpha} - u_\alpha)\Big(\frac{\delta u_\alpha}{\delta t} + c_{i\alpha}\frac{\partial u_\alpha}{\partial x_\alpha}\Big) \tag{3.3}$$

The equilibrium distribution functions f^e describe the equilibrium state of f, and are written as (He *et al.*, 1998)

$$f_{i=0,1,\dots,8}^e = \omega_i\rho\Big(1 + \frac{3\mathbf{c}_i\cdot\mathbf{u}}{c^2} + \frac{9(\mathbf{c}_i\cdot\mathbf{u})^2}{2c^4} - \frac{3\mathbf{u}^2}{2c^2}\Big)$$
$$\omega_0 = \frac{4}{9} \qquad \omega_{1,2,3,4} = \frac{1}{9} \qquad \omega_{5,6,7,8} = \frac{1}{36} \tag{3.4}$$

and

$$g_0^e = -\frac{2}{3}\rho e\Big(\frac{\mathbf{u}^2}{c^2}\Big) \qquad g_{1,2,3,4}^e = \frac{1}{9}\rho e\Big(\frac{3}{2} + \frac{3}{2}\frac{\mathbf{c}_{1,2,3,4}\cdot\mathbf{u}}{c^2} + \frac{9}{2}\frac{(\mathbf{c}_{1,2,3,4}\cdot\mathbf{u})^2}{c^4} - \frac{3}{2}\frac{\mathbf{u}^2}{c^2}\Big)$$

$$g_{5,6,7,8}^e = \frac{1}{36}\rho e\Big(3 + 6\frac{\mathbf{c}_{5,6,7,8}\cdot\mathbf{u}}{c^2} + \frac{9}{2}\frac{(\mathbf{c}_{5,6,7,8}\cdot\mathbf{u})^2}{c^4} - \frac{3}{2}\frac{\mathbf{u}^2}{c^2}\Big) \tag{3.5}$$

where $c^2 = 3RT$ and R is the constant of gas. The discretized form of Eq. $(3.1)_1$ is written as

$$f_i(\mathbf{x} + \mathbf{c}_i\Delta t, t + \Delta t) - f_i(\mathbf{x}, t) = -\frac{\Delta t}{\tau_f}[f_i(\mathbf{x}, t) - f_i^e(\mathbf{x}, t)] \tag{3.6}$$
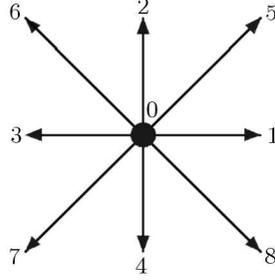

Fig. 2. D2Q9 lattice

The constant value of BGK collision operator results in the second-order truncation error in the lattice Boltzmann equation. This error is absorbed into the physical viscous term by using $\nu = (\tau_f - 0.5\Delta t)RT$ for isothermal models. But, for thermal models, the viscosity appears in both momentum and energy equations; however the viscosity in the viscous heat dissipation term of energy equation must be considered as $\nu = \tau_f RT$, which is inconsistent with the viscosity form in isothermal models. To solve this problem, a second-order strategy to integrate the Boltzmann equation is applied, which leads to the following equations – more details can be found in He *et al.* (1998) and Peng *et al.* (2003)

$$-\frac{f_i(\mathbf{x}, t) - f_i^e(\mathbf{x}, t)}{\tau_f} = -\frac{\Delta t}{2\tau_f}[f_i(\mathbf{x} + \mathbf{c}_i\Delta t, t + \Delta t) - f_i^e(\mathbf{x} + \mathbf{c}_i\Delta t, t + \Delta t)]$$

$$-\frac{\Delta t}{2\tau_f}[f_i(\mathbf{x}, t) - f_i^e(\mathbf{x}, t)]$$

$$f_i(\mathbf{x} + \mathbf{c}_i\Delta t, t + \Delta t) - f_i(\mathbf{x}, t) = -\frac{\Delta t}{2\tau_f}[f_i(\mathbf{x} + \mathbf{c}_i\Delta t, t + \Delta t) - f_i^e(\mathbf{x} + \mathbf{c}_i\Delta t, t + \Delta t)]$$

$$-\frac{\Delta t}{2\tau_f}[f_i(\mathbf{x}, t) - f_i^e(\mathbf{x}, t)] \tag{3.7}$$

Using the same procedure done on Eqs. (3.6) and (3.7) for Eq. $(3.1)_1$, the following equations are obtained for Eq. $(3.1)_2$

$$-\frac{g_i(\mathbf{x}, t) - g_i^e(\mathbf{x}, t)}{\tau_g} - f_i(\mathbf{x}, t)Z_i(\mathbf{x}, t) = -\frac{\Delta t}{2\tau_g}[g_i(\mathbf{x} + \mathbf{c}_i\Delta t, t + \Delta t) - g_i^e(\mathbf{x} + \mathbf{c}_i\Delta t, t + \Delta t)]$$

$$-\frac{\Delta t}{2}f_i(\mathbf{x} + \mathbf{c}_i\Delta t, t + \Delta t)Z_i(\mathbf{x} + \mathbf{c}_i\Delta t, t + \Delta t) - \frac{\Delta t}{2\tau_g}[g_i(\mathbf{x}, t) - g_i^e(\mathbf{x}, t)]$$

$$-\frac{\Delta t}{2}f_i(\mathbf{x}, t)Z_i(\mathbf{x}, t)$$

$$g_i(\mathbf{x} + \mathbf{c}_i\Delta t, t + \Delta t) - g_i(\mathbf{x}, t) = -\frac{\Delta t}{2\tau_g}[g_i(\mathbf{x} + \mathbf{c}_i\Delta t, t + \Delta t) - g_i^e(\mathbf{x} + \mathbf{c}_i\Delta t, t + \Delta t)] \tag{3.8}$$

$$-\frac{\Delta t}{2}f_i(\mathbf{x} + \mathbf{c}_i\Delta t, t + \Delta t)Z_i(\mathbf{x} + \mathbf{c}_i\Delta t, t + \Delta t) - \frac{\Delta t}{2\tau_g}[g_i(\mathbf{x}, t) - g_i^e(\mathbf{x}, t)]$$

$$-\frac{\Delta t}{2}f_i(\mathbf{x}, t)Z_i(\mathbf{x}, t)$$

To solve the difficulty of implicitness of Eqs. $(3.7)_2$ and $(3.8)_2$, two distribution functions $\widetilde{f}_i$ and $\widetilde{g}_i$ are defined. The symbols $\widetilde{f}$ and $\widetilde{g}$ are defined for the numerical purpose. However, they indicate the momentum and internal energy distribution functions like f and g, respectively (He $et\ al.$, 1998)

$$\widetilde{f}_i = f_i + \frac{\Delta t}{2\tau_f}(f_i - f_i^e) - \frac{\Delta t}{2}F \qquad\qquad \widetilde{g}_i = g_i + \frac{\Delta t}{2\tau_g}(g_i - g_i^e) + \frac{\Delta t}{2}f_i Z_i \qquad (3.9)$$

In each time step, the collision and propagation stages are performed sequentially between particles. In BGK model, these stages are stated as follows

$$\widetilde{f}_i(\mathbf{x} + \mathbf{c}_i\Delta t, t + \Delta t) - \widetilde{f}_i(\mathbf{x}, t) = -\frac{\Delta t}{\tau_f + 0.5\Delta t}[\widetilde{f}_i(\mathbf{x}, t) - f_i^e(\mathbf{x}, t)]$$

$$\widetilde{g}_i(\mathbf{x} + \mathbf{c}_i\Delta t, t + \Delta t) - \widetilde{g}_i(\mathbf{x}, t) = -\frac{\Delta t}{\tau_g + 0.5\Delta t}[\widetilde{g}_i(\mathbf{x}, t) - g_i^e(\mathbf{x}, t)] - \frac{\tau_g \Delta t}{\tau_g + 0.5\Delta t}f_i Z_i \qquad (3.10)$$

Finally, using $\widetilde{f}_i$ and $\widetilde{g}_i$, the hydrodynamic and thermal variables are calculated as

$$\rho = \sum_i \widetilde{f}_i \qquad\qquad \rho e = \sum_i \widetilde{g}_i - \frac{\Delta t}{2}\sum_i f_i Z_i \qquad\qquad \rho\mathbf{u} = \sum_i \mathbf{c}_i\widetilde{f}_i$$

$$\mathbf{q} = \frac{\tau_g}{\tau_g + 0.5\Delta t}\left(\sum_i \mathbf{c}_i\widetilde{g}_i - \rho e\mathbf{u} - \frac{1}{2}\Delta t\sum_i \mathbf{c}_i f_i Z_i\right) \qquad (3.11)$$

where $e = RT$ is the internal energy and $\mathbf{q} = [q_x, q_y]$ is the heat flux vector. ν and α are stated as

$$\nu = \tau_f RT \qquad\qquad \alpha = 2\tau_g RT \qquad (3.12)$$

Using the Chapman-Enskog expansion, the continuity and Navier-Stokes equations can be obtained from LBM-BGK equation (Cercignani, 1998). The characteristic velocity is assumed to be 0.1 to keep Ma < 1, so the kinematic viscosity is estimated as $\nu = \text{Re}/U_0 H$. Considering both $RT = 1/3$ and Eq. (3.12), the value of τ_f is determined. Now, the thermal diffusivity is calculated as $\alpha = \nu/\text{Pr}$, and finally by Eq. (3.12) it is found that $\tau_g = \alpha/2RT$.

3.2. Gravity effects

The Boussinesq approximation is used as $\rho = \overline{\rho}[1 - \beta(T - \overline{T})]$ where $\overline{\rho}$, $\overline{T}$ are the reference fluid density and temperature. The buoyancy force per unit mass is defined as $\mathbf{G} = \beta\mathbf{g}(T - \overline{T})$ and $F = \mathbf{G}\cdot(\mathbf{c} - \mathbf{u})f^e/RT$ in Eq. (3.13) refers to the buoyancy force effects in this problem (He $et\ al.$, 1998; Kuznik $et\ al.$, 2007)

$$\partial_t f + (\mathbf{c}\cdot\nabla)f = -\frac{f - f^e}{\tau_f} + F \qquad (3.13)$$

Now the discretized Boltzmann equation is written as follows (D'Orazio $et\ al.$, 2004)

$$\partial_t f_i + (\mathbf{c}_i\cdot\nabla)f_i = -\frac{f_i - f_i^e}{\tau_f} + \frac{\mathbf{G}\cdot(\mathbf{c}_i - \mathbf{u})}{RT}f_i^e \qquad (3.14)$$

where $\mathbf{G} = [G_x, G_y]$, $G_x = \beta|g|(T - \overline{T})\sin\gamma = G\sin\gamma$, and $G_y = \beta|g|(T - \overline{T})\cos\gamma = G\cos\gamma$. Using the same method as in Section 3.1 and by substituting $\mathbf{u} = [u, v]$ and $\mathbf{c}_i = [c_{ix}, c_{iy}]$, the following equations are obtained

$$\widetilde{f}_i(\mathbf{x} + \mathbf{c}_i\Delta t, t + \Delta t) - \widetilde{f}_i(\mathbf{x}, t) = -\frac{\Delta t}{\tau_f + 0.5\Delta t}(\widetilde{f}_i - f_i^e)$$

$$+ \left(\frac{\Delta t\tau_f}{\tau_f + 0.5\Delta t}\frac{3G(c_{ix} - u)}{c^2}f_i^e\right)\sin\gamma + \left(\frac{\Delta t\tau_f}{\tau_f + 0.5\Delta t}\frac{3G(c_{iy} - v)}{c^2}f_i^e\right)\cos\gamma \qquad (3.15)$$

Equation (3.9), which includes the external force term F, is written as the following (He *et al.*, 1998)

$$\widetilde{f}_i = f_i + \frac{\Delta t}{2\tau_f}(f_i - f_i^e) - \frac{\Delta t}{2}F \;\Rightarrow\; f_i = \frac{\tau_f \widetilde{f}_i + 0.5\Delta t f_i^e}{\tau_f + 0.5\Delta t} + \frac{0.5\Delta t \tau_f}{\tau_f + 0.5\Delta t}F$$

$$f_i = \frac{\tau_f \widetilde{f}_i + 0.5\Delta t f_i^e}{\tau_f + 0.5\Delta t} + \frac{0.5\Delta t \tau_f}{\tau_f + 0.5\Delta t}\frac{\mathbf{G}\cdot(\mathbf{c}_i - \mathbf{u})}{RT}f_i^e$$

(3.16)

Equation (3.16)$_2$ in the x and y directions is stated as

$$f_i = \frac{\tau_f \widetilde{f}_i + 0.5\Delta t f_i^e}{\tau_f + 0.5\Delta t} + \Big(\frac{0.5\Delta t \tau_f}{\tau_f + 0.5\Delta t}\frac{G(c_{ix} - u)}{RT}f_i^e\Big)\sin\gamma + \Big(\frac{0.5\Delta t \tau_f}{\tau_f + 0.5\Delta t}\frac{G(c_{iy} - v)}{RT}f_i^e\Big)\cos\gamma$$

(3.17)

Using the same procedure and considering the effects of gravity and γ, the following formulae are derived to calculate the macroscopic hydrodynamic variables

$$\rho = \sum_i \widetilde{f}_i \qquad u = \frac{1}{\rho}\sum_i \widetilde{f}_i c_{ix} + \frac{\Delta t}{2}G\sin\gamma \qquad v = \frac{1}{\rho}\sum_i \widetilde{f}_i c_{iy} + \frac{\Delta t}{2}G\cos\gamma \qquad (3.18)$$

3.3. Hydrodynamic boundary conditions

The non-equilibrium bounce back model is used to simulate the no-slip boundary condition on the walls (Zou and He, 1997). This model improves accuracy compared to the bounce back boundary condition and satisfies the zero mass flow rate at nodes on the wall. The collision occurs on the nodes located at the solid-fluid boundaries. The distribution functions are reflected in suitable directions, satisfying the equilibrium conditions (He *et al.*, 1998). As an example for the west wall, the known populations are $\widetilde{f}_0, \widetilde{f}_2, \widetilde{f}_3, \widetilde{f}_4, \widetilde{f}_6, \widetilde{f}_7$, and after collision to the wall nodes, the unknown populations will be $\widetilde{f}_1, \widetilde{f}_5, \widetilde{f}_8$. Using Eqs. (3.18), the following equations are obtained

$$\rho = \sum_i \widetilde{f}_i \;\Rightarrow\; \widetilde{f}_1 + \widetilde{f}_5 + \widetilde{f}_8 = \rho_w - (\widetilde{f}_0 + \widetilde{f}_2 + \widetilde{f}_3 + \widetilde{f}_4 + \widetilde{f}_6 + \widetilde{f}_7)$$

$$u = \frac{1}{\rho}\sum_i \widetilde{f}_i c_{ix} + \frac{\Delta t}{2}G\sin\gamma \;\Rightarrow\; \widetilde{f}_1 + \widetilde{f}_5 + \widetilde{f}_8 = \rho_w U_w + (\widetilde{f}_3 + \widetilde{f}_6 + \widetilde{f}_7) - \frac{\Delta t}{2}\rho_w G\sin\gamma$$

(3.19)

$$v = \frac{1}{\rho}\sum_i \widetilde{f}_i c_{iy} + \frac{\Delta t}{2}G\cos\gamma \;\Rightarrow\; \widetilde{f}_5 - \widetilde{f}_8 = \rho_w V_w + (-\widetilde{f}_2 + \widetilde{f}_4 - \widetilde{f}_6 + \widetilde{f}_7) - \frac{\Delta t}{2}\rho_w G\cos\gamma$$

where ρ_w and U_w are density and velocity at the wall nodes, respectively. Using the bounceback rule for the non-equilibrium part of the particle distribution normal to the boundary and Eqs. (3.4) (Zou and He, 1997) gives

$$\widetilde{f}_1 - \widetilde{f}_1^e = \widetilde{f}_3 - \widetilde{f}_3^e \;\Rightarrow\; \widetilde{f}_1 = \widetilde{f}_3 + \frac{2}{3}\rho_w U_w \qquad\qquad (3.20)$$

substituting Eq. (3.20) in Eqs. (3.19)$_{2,3}$, and then adding and subtracting the resulting equations leads to

$$\widetilde{f}_8 = \widetilde{f}_6 - \frac{\widetilde{f}_4 - \widetilde{f}_2}{2} + \frac{1}{6}\rho_w U_w - \frac{1}{2}\rho_w V_w + \frac{\Delta t}{4}\rho_w G(\cos\gamma - \sin\gamma)$$

$$\widetilde{f}_5 = \widetilde{f}_7 + \frac{\widetilde{f}_4 - \widetilde{f}_2}{2} + \frac{1}{6}\rho_w U_w + \frac{1}{2}\rho_w V_w - \frac{\Delta t}{4}\rho_w G(\cos\gamma + \sin\gamma)$$

(3.21)

Equations (3.20) and (3.21) are presented to include the effects of gravity and inclination angle for the no slip hydrodynamic boundary condition on the west wall, and the rest corresponding equations are written similarly for other walls and corners.

3.4. Thermal boundary conditions

The top lid and bottom wall of the cavity are maintained at constant but different temperatures, T_h and T_c, respectively, and the sidewalls are insulated. The general purpose thermal boundary condition (GPTBC) is used to implement the constant thermal boundary condition on the top and bottom walls. This model was developed by D'Orazio et al. (2003) and (2004), based on the non-equilibrium bounce back boundary condition of Zou and He (1997) and He et al. (1998). In this model, the unknown thermal populations are assumed to be equilibrium distribution functions with a counter slip thermal energy density $\rho e'$, which is determined so that suitable constraints are verified. For example, for the top moving lid

$$\widetilde{g}_{4,7,8} = \rho(e + e')\frac{g^e_{4,7,8}}{\rho e} \qquad \rho e' = 2\rho e + \frac{3}{2}\Delta t \sum_i f_i Z_i - 3K \tag{3.22}$$

K represents the sum of the six known thermal distribution functions of the neighboring nodes and e is the imposed thermal energy density at the wall. The GPTBC shows suitable stability and accuracy for different boundary conditions. Finally, the unknown distribution functions reflecting from the top wall $\widetilde{g}_4$, $\widetilde{g}_7$ and $\widetilde{g}_8$ are selected as follows (D'Orazio et al., 2003, 2004)

$$\widetilde{g}_7 = \left(3\rho e + \frac{3}{2}\Delta t \sum_i f_i Z_i - 3(\widetilde{g}_0 + \widetilde{g}_1 + \widetilde{g}_2 + \widetilde{g}_3 + \widetilde{g}_5 + \widetilde{g}_6)\right)(3.0 - 6U_0 + 3U_0^2)\frac{1}{36}$$

$$\widetilde{g}_4 = \left(3\rho e + \frac{3}{2}\Delta t \sum_i f_i Z_i - 3(\widetilde{g}_0 + \widetilde{g}_1 + \widetilde{g}_2 + \widetilde{g}_3 + \widetilde{g}_5 + \widetilde{g}_6)\right)\left(\frac{3}{2} - \frac{3}{2}U_0^2\right)\frac{1}{9} \tag{3.23}$$

$$\widetilde{g}_8 = \left(3\rho e + \frac{3}{2}\Delta t \sum_i f_i Z_i - 3(\widetilde{g}_0 + \widetilde{g}_1 + \widetilde{g}_2 + \widetilde{g}_3 + \widetilde{g}_5 + \widetilde{g}_6)\right)(3.0 - 6U_0 + 3.0U_0^2)\frac{1}{36}$$

Similar procedure is performed for the cold bottom wall. It is noted that for the implementation of the adiabatic boundary condition on the side walls, the condition $q_x = 0$ should be substituted for $\mathbf{q}$ in Eq. (3.11). For example for the west wall, the following equation is obtained (D'Orazio et al., 2003, 2004)

$$\sum_i c_{ix}\widetilde{g}_i = \frac{1}{2}\Delta t \sum_i c_{ix} f_i Z_i \tag{3.24}$$

Using Eqs. (3.22) and (3.24) for $i = 1, 5, 8$, the unknown distributions are selected as

$$\rho e' = 3(\widetilde{g}_6 + \widetilde{g}_3 + \widetilde{g}_7) + \frac{3}{2}\Delta t \sum_i \frac{c_{ix}}{c} f_i Z_i - \rho e \tag{3.25}$$

The Nusselt numbers along the top and bottom walls are estimated as follows

$$\mathrm{Nu}_X = -\left(\frac{\partial \theta}{\partial Y}\right)_{Y=0,1} \qquad \mathrm{Nu}_m = \frac{1}{AR}\int_0^{AR} \mathrm{Nu}_X \, dX \tag{3.26}$$

4. Results

The effects of γ and Pr on the fluid inside the inclined cavity shown in Fig. 1 with $\mathrm{Re} = 200$ at different Ri are studied using the lattice Boltzmann method. The top and bottom walls are at $Y = 1, 0$ respectively, whereas the side walls are considered at $X = 0, 3$.

4.1. Grid independency and validation

In order to obtain a grid independent solution, a grid refinement study is performed for a horizontal cavity ($\gamma = 0$). Grid independence of the results has been established in terms of Nu_m on the lid and dimensionless values of x-velocity U, y-velocity V, and temperature θ at $X = 1.5$ and $Y = 0.5$ (cavity centre) for three different grid sizes, namely 300×100, 450×150 and 600×200 lattice nodes. In Table 1, the results are reported as obtained for $Ri = 0.1$, $Re = 200$ and $Pr = 0.7$; because of small differences, the 450×150 grid is selected to continue the calculations.

To validate the computer code, three cases are examined. The first one is a benchmark numerical solution of a free convection square cavity flow with side walls at different temperatures and horizontal walls adiabatic, obtained by Davis (1983). The results for different Ra ranging from 10^4 to 10^5, and $Pr = 0.7$, are reported in Table 2 in which $V^* = \nu/Pr H$ represents the diffusion velocity. Table 2 shows the maximum horizontal velocity u_{max}/V^* at $x/L = 0.5$, the maximum vertical velocity v_{max}/V^* at $y/L = 0.5$ and their locations. Nu_m at the hot-wall also is reported. The second case is a mixed convection problem, investigated by Iwatsu *et al.* (1993); it concerns a square cavity, heated from the top moving wall and cooled from the bottom, with adiabatic sidewalls. Comparisons of U and T profiles along the vertical centreline for $Gr = 10^2$ and $Re = 400$ are shown in Fig. 3. As the last case for validation, the mixed convection of fluid flow and heat transfer in a vertical channel (x-direction) is studied, and the results are compared with those of Habchi and Acharya (1986). The right wall temperature is T_h (hot temperature) at $y = 0$ and the left wall is assumed adiabatic at $y = 1$. A hot block with length L is also attached to the right wall. The inlet fluid temperature is T_c (cold temperature). Dimensionless temperature profiles at the channel cross-section $x/L = 0.77$ for $Pr = 0.7$, $Ra = 10^5$ and different values of Ri, are presented in Fig. 4, and good agreement is seen.

Table 1. Grid study for $Ri = 0.1$, $Re = 200$, $Pr = 0.7$ at $X = 1.5$ and $Y = 0.5$

Parameters	Mesh		
	300×100	450×150	600×200
U	-0.197	-0.195	-0.194
V	0.063	0.066	0.067
θ	0.560	0.564	0.567
Nu_m	2.331	2.367	2.382

Table 2. Comparison of the maximum horizontal velocity u_{max}/V^* at $x/L = 0.5$, the maximum vertical velocity v_{max}/V^* at $y/L = 0.5$, and their locations obtained from present results with those of Davis (1983)

Ra	u_{max}/V^* and (y/L)			v_{max}/V^* and (x/L)			Nu_m		
	Present	Davis	error %	Present	Davis	error %	Present	Davis	error %
10^4	15.951 (0.817)	16.178 (0.823)	-1.403 (-0.729)	19.338 (0.123)	19.617 (0.119)	-1.422 (3.361)	2.210	2.243	-1.471
10^5	34.239 (0.851)	34.730 (0.855)	-1.414 (-0.468)	67.501 (0.067)	68.590 (0.066)	-1.588 (1.515)	4.456	4.519	-1.394

4.2. Effects of cavity inclination angle

In order to show the effects of γ on the flow field and heat transfer, in Fig. 5 streamlines and isotherms are reported at different $\gamma = 0°$, $30°$, $60°$ and $90°$ for the case $Ri = 1$ at $Pr = 0.7$,
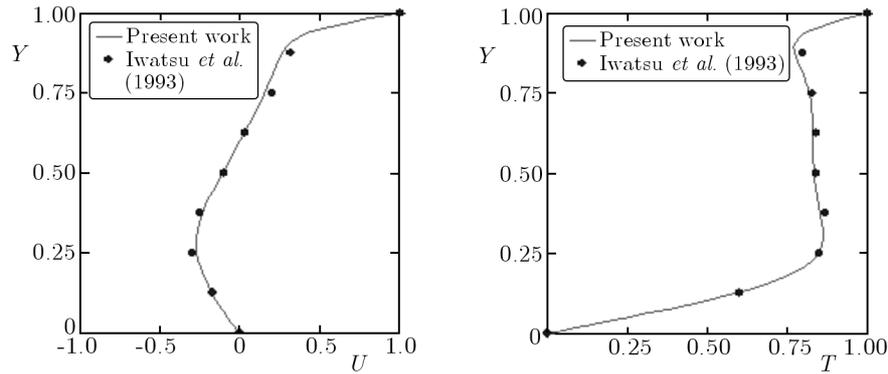
Fig. 3. Comparison of U and T along the cavity vertical centreline with Iwatsu *et al.* (1993)
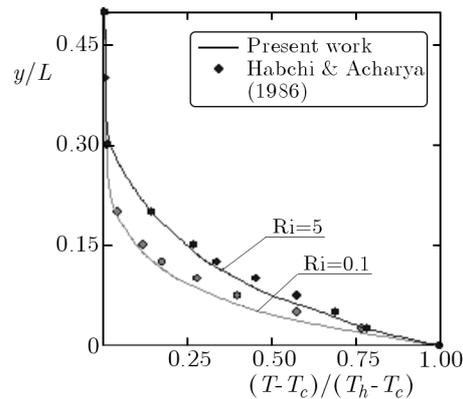

Fig. 4. Dimensionless temperature profiles with those of Habchi and Acharya (1986)

respectively. A clockwise rotational cell is produced in the fluid flow because of cavity lid motion which transports the hot fluid to the lower parts of the cavity space. The desired pressure gradient in the vertical direction is made due to such hot fluid motion and, consequently, the buoyancy forces are generated to push the hot fluid to the upper parts again. Combination of these two mechanisms of heat transfer, resulting from lid motion and buoyancy forces, is named as mixed convection. The Richardson number is defined as $\mathrm{Ri} = \mathrm{Gr}/\mathrm{Re}^2$; it means that for $\mathrm{Ri} \ll 1$ and $\mathrm{Ri} \gg 1$, the forced and free convection are the dominant heat transfer mechanisms, respectively, and for Ri 1 the mixed convection is considered.

At forced convection domination ($\mathrm{Ri} = 0.1$), there will be only one powerful cell which will covere almost all the cavity space, and the increasing γ leads to a slight increase in the power of such a cell, and no more other important effects are seen. Figure 5 shows the two cells affecting the fluid flow as $\mathrm{Ri} = 1$, however the upper one is grater than the lower one. At a larger inclination angle, these two cells merge, so that for $\gamma = 90°$, there will be a large strong cell which covers the whole cavity space. The inclination angle has significant effects on the thermal and hydrodynamic fluid parameters when natural convection dominates the cavity space. The straight isotherms, which are almost perpendicular to the sidewalls, can be seen in this case as $\gamma = 0°$, especially in the lower half of the enclosure space which shows the conduction heat transfer in this region. Figure 6 shows the dimensionless horizontal velocity profile U and dimensionless temperature profile θ along the cavity vertical centreline at $x/H = 1.5$ for $\mathrm{Ri} = 1$, $\mathrm{Pr} = 0.7$ and different inclination angles.

At $Y = 0$, U is zero and at $Y = 1$, it approaches the lid velocity. A larger γ corresponds to a larger absolute value of U at $0 < Y < 0.3$. The larger γ corresponds to the larger absolute value of U at $0 < Y < 0.3$; it means faster fluid movement in the lower part of the cavity with the
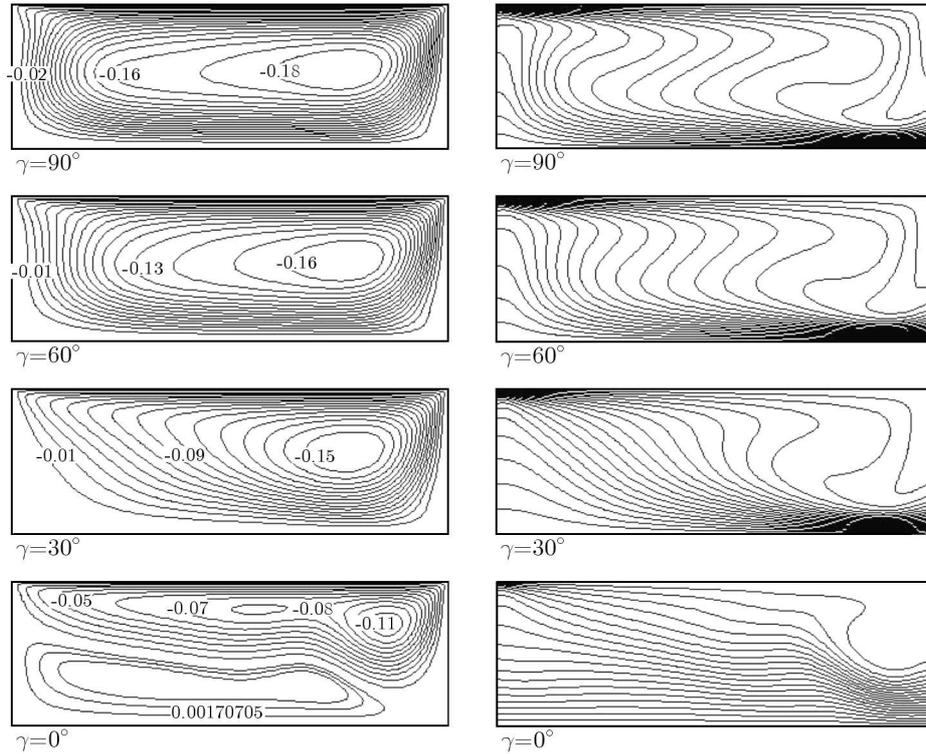
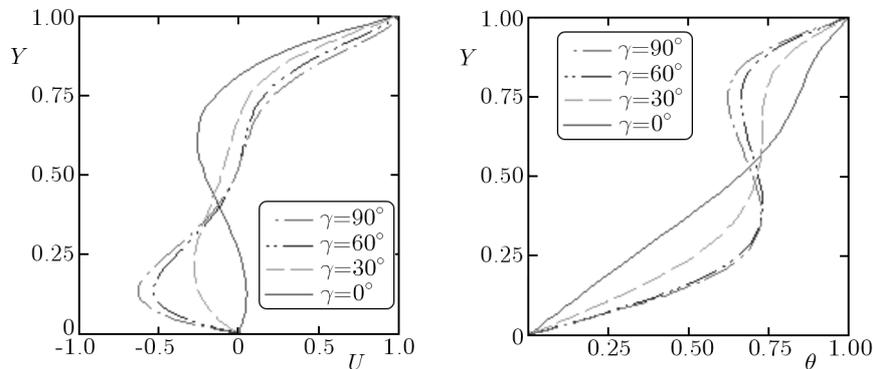Fig. 5. Streamlines (left) and isotherms (right) for Ri = 1, at $\gamma = 0°$, 30°, 60° and 90°, Pr = 0.7

Fig. 6. Profiles of U and θ at $x/H = 1.5$ for Ri = 1 and Pr = 0.7

increasing inclination angle. At $\gamma = 0$, the temperature profile changes almost linearly from zero (cold wall temperature at $Y = 0$) to the hot wall temperature at $Y = 1$. A larger inclination angle leads to less temperature differences in the central region of the cavity, which shows the core of the rotational cell. Thin thermal boundary layers along the top and bottom walls can be seen due to high temperature variations close to these walls. At $\gamma = 60°$ and $\gamma = 90°$, the temperature values at $Y = 0.3$ are higher than the corresponding values at $Y = 0.75$; however the bottom cold wall is closer to the region at $Y = 0.3$. This physical phenomenon illustrates the desired temperature gradient to generate the buoyancy forces in these regions. At higher Ri, the larger γ increases the absolute value of U adjacent to the upper and lower walls. Thus, in spite of previous articles (Iwatsu *et al.*, (1993)), the U_{max} value can be higher than the moving lid velocity (at Ri = 10 and $\gamma = 90°$). This phenomenon occurs because of the effects of both buoyancy forces and lid motion.

4.3.   Effects of Prandtl number

The effects of $Pr = 0.7$ were studied in Section 4.2, and in this section, the effects of $Pr = 0.07, 7$ are studied. Figure 7 shows the profiles of U and θ for $Ri = 0.1$ at $Pr = 7$.
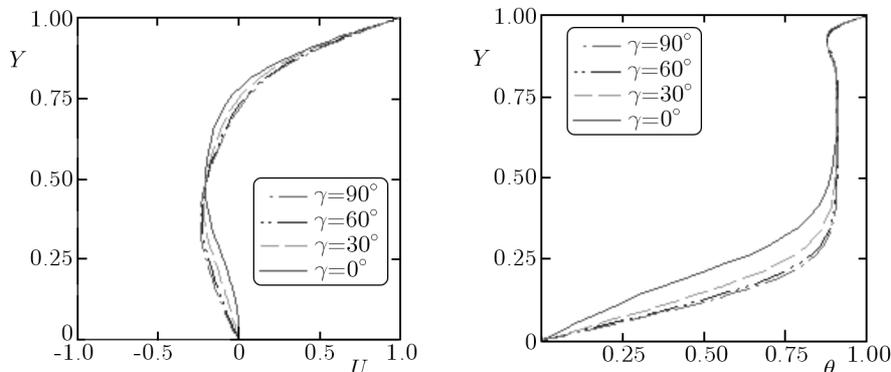

Fig. 7. Profiles of U and θ at $x/H = 1.5$ for $Ri = 0.1$ and $Pr = 7$

It is seen that the largest temperature variations occur in the lower part of the cavity ($Y < 0.25$), which is different from the related results in the previous section. This cavity space is far from the top lid, so its properties depend more on the buoyancy forces than the lid motions. The increasing γ leads to more significant effects on temperature profiles in this region. Figure 8 shows profiles of U and θ for $Ri = 10$ at $Pr = 7$. A larger Pr corresponds to a larger U_{max} in the state of natural convection dominance. Figure 9 shows Nu_m on the hot wall as a function of γ for $Ri = 0.1, 1, 10$ and $Pr = 0.07, 0.7, 7$. It has to be noted that for $\gamma = 0$, Nu_m decreases when Ri increases, it implies the weak contribution of natural convection in the horizontal configuration. With regard to $\gamma \neq 0$, for $Ri = 0.1$, Nu_m increases with γ slightly; and for $Ri \geqslant 1$ it would increase more intensively.
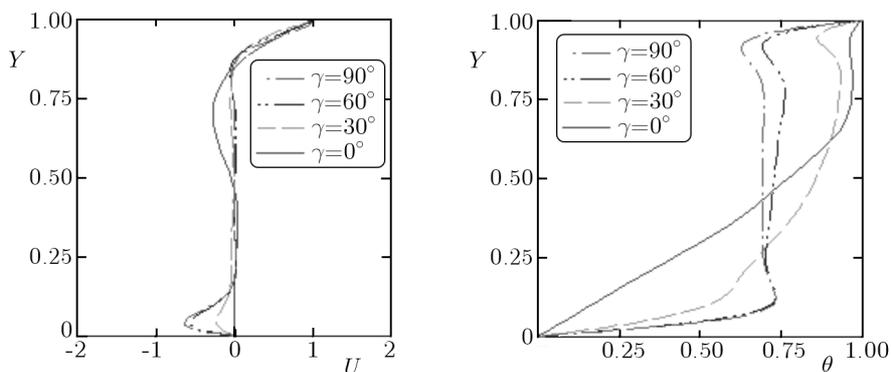

Fig. 8. Profiles of U and θ at $x/H = 1.5$ for $Ri = 10$ and $Pr = 7$

A larger Pr corresponds to a larger Nu_m, especially at higher values of Ri and γ. Nu_m at $Ri = 10$ and $Pr = 7$ increases more strongly with the increasing of $\gamma = 0°$ to $\gamma = 90°$. Moreover, for engineering applications and showing the physical effects of the parameters, the following single non-linear correlation is obtained to estimate the average Nusselt number as a function of Ri, Pr and γ, used for $0.1 \leqslant Ri \leqslant 10$, $0.07 \leqslant Pr \leqslant 7$, $0 \leqslant \gamma \leqslant \pi/2$ (γ in radians), $Re = 200$ and $AR = 3$. The average deviation of this correlation is 4.5%

$$Nu_m = 0.2364 + 2.957Ri^{0.2522}Pr^{0.3277}\gamma^{0.5074} + 1.637Ri^{-0.1629}Pr^{0.3344} - 0.8402\gamma^{0.4872} \quad (4.1)$$
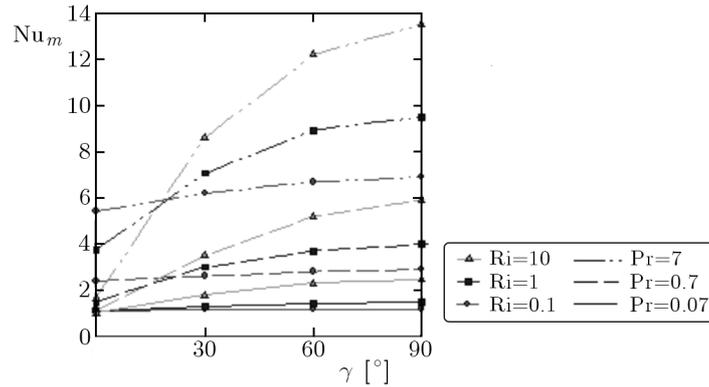
Fig. 9. Nu_m on the hot wall as a function of γ ? for different Ri and Pr

5. Conclusion

As an alternative method, a thermal LBM-BGK was developed to study the fluid mixed convection in an inclined enclosure. In this problem, gravity effects and the inclination angle changed the velocity components resulted from the moving top lid. In order to use LBM, the collision term of the Boltzmann equation and the calculation procedure of the macroscopic properties and hydrodynamic boundary conditions were modified so that the buoyancy forces and the inclination angle could be incorporated properly into the solution process. Moreover, a correlation was introduced for the average Nusselt number as a function of Ri, Pr and γ.

The results show that with increasing γ and for Pr = 0.7, the thermal and hydrodynamic flow parameters change more. For Ri = 10, $\gamma = 60°$ and $\gamma = 90°$, the absolute U adjacent to the upper and lower walls could be more than the U_0. At natural convection dominance, the variations of the inclination angle affect more the fluid flow and heat transfer rate. For the inclined cavity, at $\gamma = 0°$, the maximum value of Nu_m is obtained at Ri = 0.1, but at larger inclination angles it occurs at Ri = 10. At larger Pr values, the heat transfer rate is more sensitive to variations of γ at natural convection dominance. Nu_m increases with the increase of Pr, especially at higher values of Ri and γ. Nu_m at Ri = 10 and Pr = 7 increases more strongly (by a factor of 9) as the inclination angle increases from $\gamma = 0°$ to $\gamma = 90°$. A higher heat transfer rate occurs at larger Pr values; however, to obtain the higher value of Nu_m at $\gamma = 0°$ (horizontal cavity) and $\gamma \geqslant 30°$, the dominant mechanism of heat transfer must be forced and natural convection, respectively.

To increase the heat transfer rate in the horizontal cavity, forced convection must be the dominant heat transfer mechanism. In this state, increasing the lid velocity results in an appropriate heat transfer growth. However, for the inclined and vertical cavity, the maximum values of heat transfer occur at the state of natural convection dominance. Thus, in this state, the increase of buoyancy forces leads to the increase of heat trasfer. To achieve an increased heat transfer rate, physical geometry and fluid Pr value must be changed. A higher heat transfer rate occurs at larger Pr values. This phenomenon is significant at larger values of the inclination angles for the state of natural convection dominance. It is recommended to use the cavity in the vertical position at the state of natural convection dominance to obtain the larger heat transfer rate.

References

1. BASAK T., ROY S., SHARMA P.K., POP I., 2009, Analysis of mixed convection flows within a square cavity with linearly heated side wall(s), *Int. J. of Heat and Mass Transfer*, **52**, 2224-2242

2. Bhatnagar P.L., Gross E.P., Krook M., 1954, A model for collision process in gases. I. Small amplitude processes in charged and neutral one-component system, *Phys. Rev.*, **94**, 511-1954

3. Bogusławski L., 2007, Estimation of the influence of inflow turbulence on heat convection from a sphere surface, *Journal of Theoretical and Applied Mechanics*, **45**, 505-511

4. Buick J.M., Greated C.A., 2000, Gravity in a lattice Boltzmann model, *Phys. Review E*, **61**, 5307-5319

5. Cercignani C., 1988, The Boltzmann Equation and its Applications, Applied Mathematical Sciences 67, Springer-Verlag, New York

6. Chen H., Chen S., Mathaaeus W.M., 1992, Recovery of the Navier-Stokes equations using a lattice-gas Boltzmann method, *Physical Review A*, **45**, 5339-5342

7. Chen S., Doolen G., 1998, Lattice Boltzmann method for fluid flows, *Annual Rev. Fluid Mech.*, **30**, 329-364

8. Cheng M., Hung K.C., 2002, Lattice Boltzmann method on nonuniform mesh, *Recent Advances in Computational Science And Engineering*, 196-199

9. Davis G.V., 1983, Natural convection of air in a square cavity: a benchmark numerical solution, *Int. J. Numer. Methods Fluids*, **3**, 249-264

10. D'Orazio A., Corcione M., Celata G., 2004, Application to natural convection enclosed flows of a lattice Boltzmann BGK model coupled with a general purpose thermal boundary condition, *Int. J. of Thermal Science*, **43**, 575-586

11. D'Orazio A., Succi S., Arrighetti C., 2003, Lattice Boltzmann simulation of open flows with heat transfer, *Phys. of Fluids*, **15**, 2778-2780

12. Du H.Y., Chai Z.H., Shi B.C., 2011, Lattice Boltzmann study of mixed convection in a cubic cavity, *Commun. Theor. Phys.*, **56**, 144-150

13. Fattahi E., Farhadi M., Sedighi K., 2011, Lattice Boltzmann simulation of mixed convection heat transfer in eccentric annulus, *Int. Communications in Heat and Mass Transfer*, **38**, 1135-1141

14. Grucelski A., Pozorski J., 2012, Lattice Boltzmann simulation of fluid flow in porous media of temperature-affected geometry, *Journal of Theoretical and Applied Mechanics*, **50**, 193-214

15. Guo Y., Bennacer R., Shen S., Ameziani D., Bouzidi M., 2010, Simulation of mixed convection in slender rectangular cavity with lattice Boltzmann method, *Int. J. of Numerical Methods for Heat and Fluid Flow*, **20**, 130-148

16. Guo Z., Zheng C., Shi B., Zhao T.S., 2007, Thermal lattice Boltzmann equation for low Mach number flows: Decoupling model, *Phys. Rev. E*, **75** (036704) 1-15

17. Habchi S., Acharya S., 1986, Laminar mixed convection in a partially blocked, vertical channel, *Int. J. Heat Mass Transfer*, **29**, 1711-1722

18. He X., Luo L.S., 1997, Lattice Boltzmann Model for the Incompressible Navier-Stokes Equation, *J. of Statistical Phys.*, **88**, 927-944

19. He X., Chen S., Doolen G., 1998, A novel thermal model for the lattice Boltzmann method in incompressible limit, *J. of Comp. Phys.*, **146**, 282-300

20. Iwatsu R., Hyun J.M., Kuwahara K., 1993, Mixed convection in a driven cavity with a stable vertical temperature gradient, *Int. J. Heat Mass Transfer*, **36**, 1601-1608

21. Jafari M., Naysari A., Bodaghi K., 2011, Lattice Boltzmann Simulation of Natural Convection Heat Transfer in an Inclined Open Ended Cavity, *World Academy of Science Engineering and Technology*, **78**, 493-498

22. Kandlikar S.G., Garimella S., Li D., Colin S., King M., 2006, *Heat Transfer and Fluid Flow in Minichannels and Microchannels*, First ed., Britain: Elsevier

23. Kao P.H., Yang R.J., 2007, Simulating oscillatory flows in Rayleigh-Bénard convection using the lattice Boltzmann method, *Int. J. of Heat and Mass Transfer*, **50**, 3315-3328

24. KAO P.H., YANG R.J., 2008, An investigation into curved and moving boundary treatments in the lattice Boltzmann method, *Journal of Computational Physics*, **227**, 5671-5690

25. KARIMIPOUR A., HOSSEIN NEZHAD A., D'ORAZIO A., SHIRANI E., 2012, Investigation of the gravity effects on the mixed convection heat transfer in a microchannel using lattice Boltzmann method, *Int. Journal of Thermal Sciences*, **54**, 142-152

26. KEFAYATI GH.R., HOSSEINIZADEH S.F., GORJI M., SAJJADI H., 2011, Lattice Boltzmann simulation of natural convection in tall enclosures using water/SiO$_2$ nanofluid, *Int. Communications in Heat and Mass Transfer*, **38**, 798-805

27. KUZMIN A., MOHAMAD A., 2009, *Multiphase Simulations with Lattice Boltzmann Scheme*, Ph.D. thesis, University of Calgary, Alberta

28. KUZNIK F., VAREILLES J., RUSAOUEN G., KRAUSS G., 2007, A double-population lattice Boltzmann method with non-uniform mesh for the simulation of natural convection in a square cavity, *International Journal of Heat and Fluid Flow*, **28**, 862-870

29. MEZRHAB A., JAMI M., ABID C., BOUZIDI M., LALLEMAND P., 2006, Lattice-Boltzmann modelling of natural convection in an inclined square enclosure with partitions attached to its cold wall, *Int. J. of Heat and Fluid Flow*, **27**, 456-465

30. MOHAMAD A.A., 2011, *Lattice Boltzmann Method Fundamentals and Engineering Applications with Computer Codes*, Springer, Canada

31. NEMATI H., FARHADI M., SEDIGHI K., FATTAHI E., DARZI A.A.R., 2010, Lattice Boltzmann simulation of nanofluid in lid-driven cavity, *Int. Communications in Heat and Mass Transfer*, **37**, 1528-1534

32. NIU X.D., SHU C., CHEW Y.T., 2007, A thermal lattice Boltzmann model with diffuse scattering boundary condition for micro thermal flows, *Comput. Fluids*, **36**, 273-281

33. ORAN E.S., OH C.K., CYBYK B.Z., 1998, Direct simulation Monte Carlo: recent advances and applications, *Ann. Rev. Fluid Mech.*, **30**, 403-441

34. PARMIGIANI A., HUBER C., CHOPARD B., LATT J., BACHMANN O., 2009, Application of the multi distribution function lattice Boltzmann approach to thermal flows, *Eur. Phys. J. Special Topics*, **171**, 37-43

35. PENG, Y., SHU, C., CHEW, Y.T., 2003, Simplified thermal lattice Boltzmann model for incompressible thermal flows, *Physical Review E*, **68**, 026701-1-8

36. PENG G., XI H., DUNCAN C., CHOU S.H., 1999, Finite volume scheme for the lattice Boltzmann method on unstructured meshes, *Phys. Rev. E*, **59**, 4675-4682

37. QIAN Y., HUMIÈRES D., LALLEMAND P., 1992, Lattice BGK models for Navier-Stokes equation, *Europhys. Lett.*, **17**, 479-484

38. ROSDZIMIN A.R.M., ZUHAIRI S.M., AZWADI C.S.N., 2010, Simulation of mixed convective heat transfer using lattice Boltzmann method, *Int. J. of Automotive and Mechanical Engineering*, **2**, 130-143

39. SHARIF M.A.R., 2007, Laminar mixed convection in shallow inclined driven cavities with hot moving lid on top and cooled from bottom, *Applied Thermal Engineering*, **27**, 1036-1042

40. SHI Y., ZHAO T.S., GUO Z.L., 2006, Lattice Boltzmann method for incompressible flows with large pressure gradients, *Phys. Review E*, **73**, 026704-1-11

41. SIVASANKARAN S., SIVAKUMAR V., PRAKASH P., 2010, Numerical study on mixed convection in a lid-driven cavity with non-uniform heating on both sidewalls, *Int. J. of Heat and Mass Transfer*, **53**, 4304-4315

42. TALLAVAJHULA A., KHARAGPUR I., RUEDE U., BARTUSCHAT D., 2011, *Introduction to the Lattice Boltzmann Method*, 10th Indo-German Winter Academy

43. TIAN Z., CHEN S., ZHENG C.G., 2010, Lattice Boltzmann simulation of gaseous finite-Knudsen microflows, *Int. J. Mod. Phys.*, **21**, 769-783

44. UBERTINI S., SUCCI S., 2008, A generalised lattice Boltzmann equation on unstructured grids, *Communications in Computational Physics*, **3**, 342-356

45. YANG Y.T., LAI F.H., 2011, Numerical study of flow and heat transfer characteristics of alumina-water nanofluids in a microchannel using the lattice Boltzmann method, *Int. Communications in Heat and Mass Transfer*, **38**, 607-614

46. ZOU Q., HE X., 1997, On pressure and velocity boundary conditions for the lattice Boltzmann BGK model, *Phys. Fluids*, **9**, 1591-1598

Analiza za pomocą siatki Boltzmanna wpływu kąta pochylenia oraz liczby Prandtla na mieszaną konwekcję w ukośnej szczelinie domkniętej ruchomą pokrywą

Streszczenie

W pracy zajęto się problemem mieszanej konwekcji laminarnej w dwuwymiarowej, prostokątnej i ukośnie usytuowanej szczelinie domkniętej od góry ruchomą pokrywą. W badaniach zastosowano metodę siatki termicznej Boltzmanna (LBM) podwójnej populacji, uwzględniając różne wartości liczby Richardsona, kąta pochylenia szczeliny oraz liczby Prandtla. W rozważanym zagadnieniu, składowe prędkości zostały poddane zmianom indukowanym siłami wyporu oraz kątem pochylenia szczeliny. Porównanie otrzymanych wyników analizy z dostępnymi w literaturze danymi wykazało dobrą zgodność. Rezultatem badań w pracy są także profile rozkładu prędkości i temperatury, liczba Nusselta, linie prądu oraz izotermy, które szczegółowo przedyskutowano. Pokazano, że wzrost liczby Prandtla zwiększa transfer ciepła, zwłaszcza dla wyższych wartości kąta pochylenia szczelin i liczby Richardsona. Co więcej, średnia liczba Nusselta przy górnych wartościach przyjętego zakresu zmienności liczb Richardsona i Prandtla wzrasta 9-krotnie.